JOURNAL OF SOLID STATE CHEMISTRY **128,** 142–149 (1997)
ARTICLE NO. SC967194

A Raman Study of New Phospho-silicides: $RhSi_3P_3$ and $IrSi_3P_3$

J. Kreisel,* O. Chaix-Pluchery,*,[1] F. Genet,† G. Lucazeau,† H. Vincent,* and R. Madar*

*Laboratoire des Matériaux et du Génie Physique (CNRS UMR 5628), ENSPG, INPG, B.P. 46, 38402 St. Martin d'Hères Cedex, France; and †Laboratoire d'Electrochimie et de Physicochimie des Matériaux et des Interfaces (CNRS UMR 5631), ENSEEG, INPG, B.P. 75, 38402 St. Martin d'Hères Cedex, France

Received February 12, 1996; in revised form October 14, 1996; accepted October 17, 1996

Raman spectra of single crystals of new phospho-silicides $RhSi_3P_3$ and $IrSi_3P_3$ confirm that the compounds crystallize in the monoclinic system, space group $C2$, which unambiguously attests to a noncentrosymmetric structure. Polarized Raman spectra of both isomorphous compounds have been measured and normal mode calculations performed at the Brillouin zone center. A very good agreement between observed and calculated wavenumbers has been obtained and allows all optical modes to be assigned. The optical vibrations have been described in terms of the potential energy distribution and of the Cartesian displacements of the atoms. © 1997 Academic Press

INTRODUCTION

Many binary transition metal silicides and phosphides have been prepared and investigated (1). The great interest in these materials has been motivated by the variety of their physical properties (1, 2) and their practical importance in Si-based microelectronics. Since phosphorus is generally used as a dopant in Si-semiconductor technology, it is of great interest to gain a better understanding of ternary phases which may result from the combination of silicon and phosphorus with a transition metal. Recently, the synthesis and crystal structure of new transition metal phospho-silicides MSi_xP_y have been reported (M = Fe, Co, Ru, Rh, Os, Ir, Pt) (3–6). All of these compounds crystallize in noncentered groups, although some of them, especially $RhSi_3P_3$ and $IrSi_3P_3$, crystallize in a pseudo-centered structure. In the present work, $RhSi_3P_3$ and $IrSi_3P_3$ will be analyzed and characterized by Raman spectroscopy and normal mode calculations to get a better knowledge of their structural and physical properties. It is worth mentioning that just a few works about vibrational spectra of transition metal silicides and phosphides have been published up to now (7–11), while no paper concerning the phospho-silicides has been published. Finally, in view of the *in situ* Raman control of silicide films obtained during CVD process (12), the present results contribute to the data bank collected on such silicon compounds.

EXPERIMENTAL AND STRUCTURE

Samples

The single crystals of $RhSi_3P_3$ and $IrSi_3P_3$ were synthesized by flux technique, where the solvent material was liquid tin as mentioned for the synthesis of transition metal silicides (13). The starting elemental materials of high purity rhodium or iridium (99.9%), red phosphorus in grains (99.9%), crushed silicon powder (99.9%), and tin, in proportions 1:3:3:6, were sealed in evacuated silica tubes and heated at 1050°C for 12 h.

Raman Spectroscopy

Raman spectra were collected using a Dilor XY multichannel spectrometer, equipped with a microscope. The 514.5 nm line of an Ar^+ ion laser was used as the excitation line. Experiments were conducted in micro-Raman; the light was focused to a 1 μm^2 spot. In these experiments, the laser powers actually taken into account are those measured at the surface of the sample. We have verified that laser powers up to 11.5 mW did not produce significant damage to the sample. Standard experiments have been carried out using incident powers ranging from 3.6 to 10.4 mW. The so-called "unpolarized" Raman spectra were collected without analyzer on the scattered beam. The polarized spectra were recorded under different polarization configurations (polarizer + analyzer). Because the orientation of the samples is not accurately known, the crystal position was modified until the best polarization contrast was obtained. All measurements performed under the microscope were recorded in a backscattering geometry, including polarized Raman measurements. The instrumental resolution was $2.8 \pm 0.2\ cm^{-1}$.

[1] To whom correspondence should be addressed.

0022-4596/97 $25.00

Crystal Structure

As concluded from diffraction measurements, $RhSi_3P_3$ and $IrSi_3P_3$ crystallize in the monoclinic system; the symmetry group may be the noncentrosymmetric space group $C2$ (or C_2^3) or the centrosymmetric $C2/m$ (or C_{2h}^3), with two formula units per unit cell. Nevertheless, refinements of the structure performed for both space groups lead to better results in the noncentrosymmetric case (3). The lattice constants are $a = 6.626$ Å, $b = 7.210$ Å, $c = 5.522$ Å, and $\beta = 118.31°$ for $RhSi_3P_3$ and $a = 6.577$ Å, $b = 7.229$ Å, $c = 5.484$ Å, and $\beta = 117.91°$ for $IrSi_3P_3$. The PSi1 and PSi2 atoms are located in a general position for both space groups. The Si atom is in a general position for the $C2$ space group and its site symmetry is m for the $C2/m$ group. The Ir and Rh atoms are in special positions; their site symmetries are 2 for the $C2$ group and $2/m$ for the $C2/m$ one.

The structure can be described by octahedra of Si or P atoms surrounding Rh or Ir metallic atoms (3). The octahedra are connected to each other by Si–Si, Si–P, and P–P bonds. The P and Si atoms are fourfold coordinated. The Si site is found completely occupied by Si and the two PSi1 and PSi2 nonmetallic sites by Si and P atoms in 1 : 3 proportion. Figures 1a and 1b show the projection of the crystal structure parallel to [010] and to [001], respectively. Figure 2 represents the octahedral and tetrahedral environments of M, Si, PSi1, and PSi2 atoms. The first number appearing on the atoms of Fig. 1 and Fig. 2 is the index of the symmetry operation which gives rise to the atom; the symmetry operations are numbered according to the $C2$ space group table in "International Tables of Crystallography" (14). The second number is the index of the primitive cell to which the atoms belong. In the following, these indices are separated by a comma. For example, an atom numbered 1,1 is obtained using the identity operation and is located in the first primitive cell.

Normal Mode Calculation Method

Normal mode calculations have been performed at the zone center ($k = 0$) using a valence force field. The method first needs a structural model usually obtained by diffraction studies. It allows the description of the atomic motions in the primitive cell in terms of internal coordinates, bond stretching, angle bending, and the construction of the kinetic energy matrix G (Wilson method (15)) from these coordinates. The second type of data needed are the force

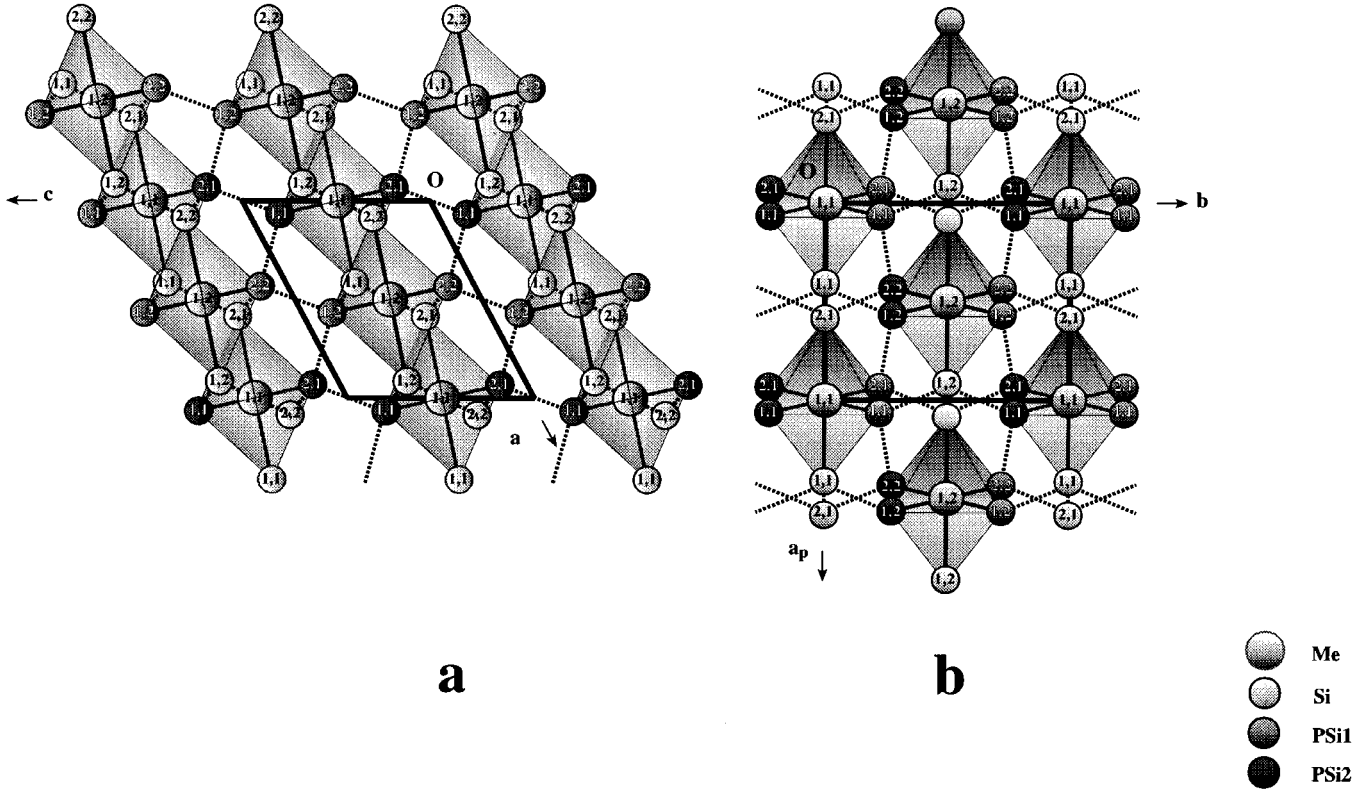

FIG. 1. Projection of $RhSi_3P_3$ and $IrSi_3P_3$ crystal structure parallel to [010] (**a**) and parallel to [001] (**b**). The indices are explained in the text.

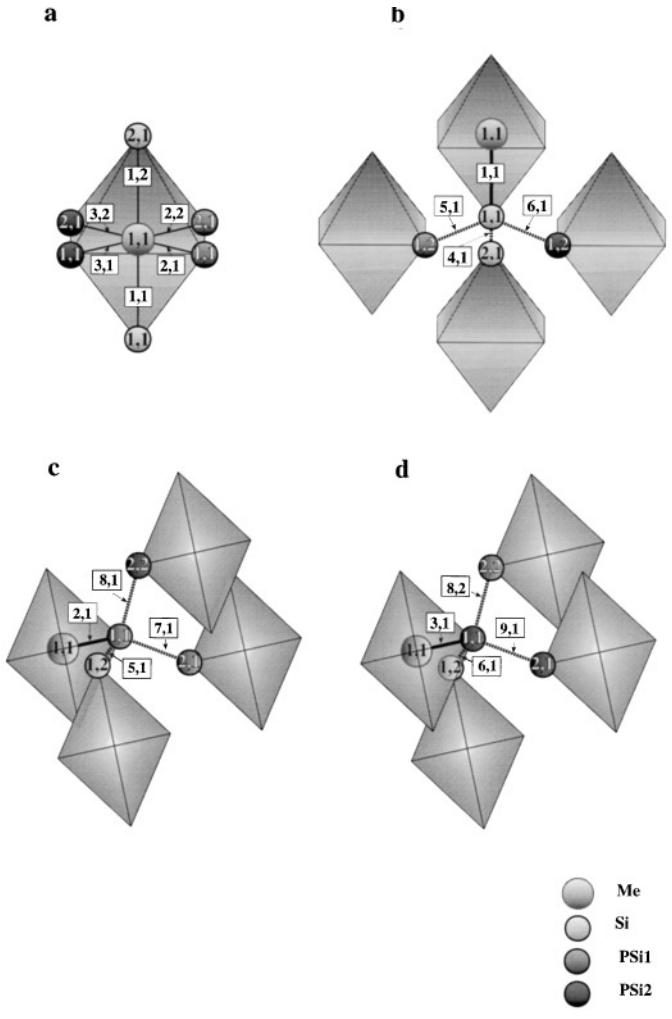

FIG. 2. Representation and numbering of bond stretching coordinates in the octahedron (**a**) and in the tetrahedral environments of Si (**b**), PSi1 (**c**), and PSi2 (**d**) atoms (**a**, **b**, projection parallel to [001]; **c**, **d** projection parallel to [010]).

constants associated with each internal coordinate. They allow the construction of the potential energy matrix F. The vibrational wavenumbers and the Cartesian displacements of the atoms involved in the corresponding vibrations are obtained from eigenvalues and eigenvectors of the GF matrix. The force constants are adjusted from comparisons between observed and calculated wavenumbers (Table 1).

The calculations have been carried out with the NORMOD program (16).The structural data for $RhSi_3P_3$ and $IrSi_3P_3$ including distribution of Si and P atoms, come from reference (3). The internal coordinates introduced in the calculations for bond stretching are the *M*–Si or *M*–PSi bonds inside the octahedron and the Si–Si, Si–PSi, and PSi–PSi bonds which link the octahedra to each other (Fig. 2). For angle bending, the internal coordinates are deformations of octahedra angles and tetrahedra angles. A first calculation using arbitrary force constants was rather promising but showed some systematic discrepancies which could be eliminated only by considering some bond–bond interaction force constants. A total of 63 different force constants (9 bond stretching, 27 angle bending, and 27 bond–bond interactions) were introduced. The final force constants found for $RhSi_3P_3$ and $IrSi_3P_3$ are given in Tables 2–4.

RESULTS AND DISCUSSION

Irreducible Representations and Space Group

Since the centrosymmetry in Rh and Ir phospho-silicides cannot be completely ascertained by diffraction methods, we have calculated the total irreducible representation by the correlation method for both possible space groups (C_2^3 and C_{2h}^3) to obtain selection rules and interpret the experimental spectra. Assuming that the structure can be described by the C_2^3 space group, the 7 atoms in the primitive cell give rise to 18 ($9A + 9B$) optical vibrational modes. All of these modes are Raman- and IR-active. On the other hand, with the C_{2h}^3 space group, 9 ($5A_g + 4B_g$) Raman-active modes and 9 ($4A_u + 5B_u$) IR-active modes are expected.

The unpolarized Raman spectra (Fig. 3), obtained from a single crystal, have shown that $RhSi_3P_3$ and $IrSi_3P_3$ crystallize in a noncentrosymmetric structure. This is evidenced by the presence of at least 18 peaks, whereas only 9 Raman bands are expected in the centrosymmetric case. The band assignment has been made by comparing polarized and unpolarized spectra. As will be discussed further a comparison of the spectra of the isomorphous compounds $RhSi_3P_3$ and $IrSi_3P_3$ based on mass effect is not valid. In the $Z(XY)\bar{Z}$ polarization configuration one observes only the *B* modes (Fig. 3). As shown in Table 1, the symmetry of the modes has been unambiguously determined for 15 of the 18 observed lines, the nonassigned bands being the three highest frequency modes. The analysis of a great number of spectra shows that additional weak lines are probably due to impurities.

Normal Mode Calculation Results

Wavenumbers. Because the symmetry of the three highest modes (Table 1) cannot be obtained unambiguously from polarization analysis, two different sets of force constants were necessary to reproduce the two possible assignments. Independent calculations have been performed for both sets. Table 1 reports for $RhSi_3P_3$ the wavenumbers calculated with both sets. The agreement between observed and calculated wavenumbers is excellent for both sets; it is slightly better for the second set. In the following, we only retain the results relative to the second set.

TABLE 1
Observed and Calculated Wavenumbers of Raman-Active Modes of $RhSi_3P_3$ and $IrSi_3P_3$ at 300 K

	$RhSi_3P_3$						$IrSi_3P_3$			
			1st set		2nd set				2nd set	
	(1)	(2)	(3)	(4)	(3)	(4)	(1)	(2)	(3)	(4)
1	202	*B*	*B*	203	*B*	203	195	*B*	*B*	195
2	210	*B*	*B*	213	*B*	212	215	*B*	*B*	213
3	228	*A* and *B*	*A*	225	*A*	225	230	*A* and *B*	*A*	222
4			*B*	233	*B*	230			*B*	230
5	245	*B*	*B*	247	*B*	245	248	*B*	*B*	250
6	273	*A*	*A*	276	*A*	279	282	*A*	*A*	279
7	289	*B*	*B*	285	*B*	288	303	*B*	*B*	301
8	295	*A*	*A*	296	*A*	295	307	*A*	*A*	306
9	400	*B*	*B*	399	*B*	399	416	*B*	*B*	416
10	415	*A*	*A*	416	*A*	417	426	*A*	*A*	426
11	433	*B*	*B*	434	*B*	435	437	*B*	*B*	434
12	454	*A*	*A*	453	*A*	452	451	*A*	*A*	451
13	473	*A*	*A*	473	*A*	472	473	*A*	*A*	483
14	489	*A*	*A*	488	*A*	488	487	*A*	*A*	488
15	493	*B*	*B*	492	*B*	492	497	*B*	*B*	495
16	498	*A* or *B*	***B***	505	***A***	504	504	*A* or *B*	***A***	505
17	537	*A* and *B*	***A***	528	***B***	530	(547)	*A* and *B*	***B***	547
18			***A***	542	***B***	538	554		***A***	554

Note. Columns (1–4) represent the following:
(1) Observed wavenumber, cm^{-1}; (2) Symmetry of mode, obtained from polarized spectra analysis; (3) Symmetry of mode, for spectra simulation; (4) Calculated wavenumber, cm^{-1}.

Potential energy distribution (*PED*). The potential energy distribution (PED) allows an estimate of the contribution of each force constant to the vibrational wavenumbers. The contributions of bond stretching and angle bending coordinates for $IrSi_3P_3$ are shown in Fig. 4. Three sets of vibration modes can be identified.

The three lowest modes depend only on bending coordinates ($n = 10$ to 36). The 195 cm^{-1} mode involves mainly bending motions in the metal octahedron and the 222 cm^{-1} mode involves bending motions localized in the PSi1 and PSi2 tetrahedra.

In the second group of modes (230 to 416 cm^{-1}), the stretching coordinates involving the silicon atom and metal atom ($n = 1$ to 3) have the most important contribution; the 301 cm^{-1} *B* mode is nearly a pure metal–silicon (*M*–Si) stretching motion.

The third group (426 to 554 cm^{-1}) corresponds mainly to stretching motions in which the metal is not involved; the

TABLE 2
Bond Stretching Force Constants of $RhSi_3P_3$ and $IrSi_3P_3$

		$RhSi_3P_3$		$IrSi_3P_3$	
n		Bond length (10^{-1} nm)	Force constants (N/cm)	Bond length (10^{-1} nm)	Force constants (N/cm)
1	$M_{1,1}$–$Si_{1,1}$	2.475	0.93	2.461	1.05
2	$M_{1,1}$–$PSi1_{1,1}$	2.371	1.50	2.373	1.52
3	$M_{1,1}$–$PSi2_{1,1}$	2.390	1.68	2.383	2.05
4	$Si_{1,1}$–$Si_{2,1}$	2.296	1.35	2.297	1.33
5	$Si_{1,1}$–$PSi1_{1,2}$	2.275	1.55	2.282	1.63
6	$Si_{1,1}$–$PSi2_{1,2}$	2.291	1.30	2.273	1.33
7	$PSi1_{1,1}$–$PSi1_{2,1}$	2.248	1.50	2.231	1.40
8	$PSi1_{1,1}$–$PSi2_{2,2}$	2.248	1.50	2.234	1.79
9	$PSi2_{1,1}$–$PSi2_{2,1}$	2.234	1.47	2.233	1.43

TABLE 3
Angle Bending Force Constants of $RhSi_3P_3$ and $IrSi_3P_3$

			$RhSi_3P_3$		$IrSi_3P_3$	
	n		Angles (°)	Force constants (N/cm rad^2)	Angles (°)	Force constants (N/cm rad^2)
M	10	$Si_{1,1}$–$M_{1,1}$–$Si_{2,1}$	178.80	0.00	179.83	0.00
(octahedral)	11	$Si_{1,1}$–$M_{1,1}$–$PSi1_{1,1}$	90.30	0.95	89.30	1.14
	12	$Si_{1,1}$–$M_{1,1}$–$PSi1_{2,1}$	88.87	0.55	90.82	0.55
	13	$Si_{1,1}$–$M_{1,1}$–$PSi2_{1,1}$	89.57	0.50	89.19	0.50
	14	$Si_{1,1}$–$M_{1,1}$–$PSi2_{2,1}$	91.23	1.11	90.69	1.11
	15	$PSi1_{1,1}$–$M_{1,1}$–$PSi1_{2,1}$	93.48	0.30	94.30	0.30
	16	$PSi1_{1,1}$–$M_{1,1}$–$PSi2_{1,1}$	85.28	0.65	86.02	0.65
	17	$PSi1_{1,1}$–$M_{1,1}$–$PSi2_{2,1}$	178.00	0.00	179.68	0.00
	18	$PSi2_{1,1}$–$M_{1,1}$–$PSi2_{2,1}$	96.00	0.30	93.67	0.30
PSi1	19	$M_{1,1}$–$PSi1_{1,1}$–$Si_{1,2}$	110.07	1.05	108.97	1.05
(tetrahedral)	20	$M_{1,1}$–$PSi1_{1,1}$–$PSi1_{2,1}$	129.32	0.17	127.86	0.30
	21	$M_{1,1}$–$PSi1_{1,1}$–$PSi2_{2,2}$	115.15	0.00	116.49	0.00
	22	$Si_{1,2}$–$PSi1_{1,1}$–$PSi1_{2,1}$	99.24	0.10	97.87	0.10
	23	$Si_{1,2}$–$PSi1_{1,1}$–$PSi2_{2,2}$	106.01	0.00	107.25	0.20
	24	$PSi1_{2,1}$–$PSi1_{1,1}$–$PSi2_{2,2}$	93.98	0.10	95.64	0.10
PSi2	25	$M_{1,1}$–$PSi2_{1,1}$–$Si_{1,2}$	106.81	1.12	109.21	1.00
(tetrahedral)	26	$M_{1,1}$–$PSi2_{1,1}$–$PSi1_{2,2}$	116.92	0.00	116.41	0.00
	27	$M_{1,1}$–$PSi2_{1,1}$–$PSi2_{2,1}$	127.09	0.40	127.66	0.35
	28	$Si_{1,2}$–$PSi2_{1,1}$–$PSi1_{2,2}$	108.06	0.00	107.33	0.10
	29	$Si_{1,2}$–$PSi2_{1,1}$–$PSi2_{2,1}$	97.41	0.00	97.90	0.00
	30	$PSi2_{2,1}$–$PSi2_{1,1}$–$PSi1_{2,2}$	98.04	0.10	95.59	0.10
Si	31	$M_{1,1}$–$Si_{1,1}$–$Si_{2,1}$	128.43	0.43	127.49	0.43
(tetrahedral)	32	$M_{1,1}$–$Si_{1,1}$–$PSi1_{1,2}$	106.94	0.00	108.75	0.00
	33	$M_{1,1}$–$Si_{1,1}$–$PSi2_{1,2}$	109.62	0.30	108.66	0.30
	34	$Si_{2,1}$–$Si_{1,1}$–$PSi1_{1,2}$	95.62	0.40	95.34	0.30
	35	$Si_{2,1}$–$Si_{1,1}$–$PSi2_{1,2}$	95.54	0.50	95.33	0.50
	36	$PSi1_{1,2}$–$Si_{1,1}$–$PSi2_{1,2}$	121.64	0.30	122.05	0.30

A and *B* modes, at 495 and 554 cm^{-1}, are mainly dependent on the PSi1–PSi2 stretching coordinate ($n = 8$).

Comparison between $IrSi_3P_3$ and $RhSi_3P_3$ force constants associated with the same internal coordinate. Force constants obtained for $IrSi_3P_3$ are on the average larger than those obtained for $RhSi_3P_3$. As a consequence, the observed frequency shifts upon Rh/Ir replacement are not attributable to a simple mass effect as would be the case for a pure isotopic substitution. Actually, three modes numbered from 7 to 9 (Table 1) described as M–X (X = Si, PSi1, or PSi2) stretching modes (Fig. 4) have larger wavenumbers for the iridium compound. This is strictly inverse of what is expected from the mass effect. Under these conditions, it is not surprising to find associated force constants larger for the iridium compound. On the other hand, X–X stretching force constants are found to be quite similar in both compounds. This shows that the nature of the metal is responsible for the M–X force constant increase from $RhSi_3P_3$ to $IrSi_3P_3$. The spatial extension of 5*d* orbitals for iridium is larger than the 4*d* orbitals in rhodium. Thus the overlap between metal orbitals and silicon orbitals, keeping constant the internuclear distances, is larger for the iridium compound and this could explain the force constant increase.

Comparison between the different stretching force constants for each compound. One finds that the force constants associated with stretching coordinates involving atoms of the same nature separated by practically equal distances are actually quite different. As an example, for $IrSi_3P_3$, the PSi1–PSi1, PSi1–PSi2, and PSi2–PSi2 force constants ($n =$ 7, 8, and 9 in Table 2) are 1.40, 1.79, and 1.43 Nm^{-1}, respectively, while interatomic distances are 0.2231, 0.2234, and 0.2233 nm, respectively. Chemical environments of PSi1 and PSi2 atoms are identical. Bonds 7 and 9 play the same role in the structure: they insure the connection between M–X octahedra located in the same plane

TABLE 4
Bond–bond Interaction Force Constants of $RhSi_3P_3$ and $IrSi_3P_3$

	n			$RhSi_3P_3$	$IrSi_3P_3$
				Force constants (N/cm)	
M	37	$M_{1,1}$–$Si_{1,1}$	$M_{1,1}$–$Si_{2,1}$	0.20	0.00
(octahedral)	38	$M_{1,1}$–$Si_{1,1}$	$M_{1,1}$–$PSi1_{1,1}$	0.00	0.00
	39	$M_{1,1}$–$Si_{1,1}$	$M_{1,1}$–$PSi1_{2,1}$	− 0.20	0.00
	40	$M_{1,1}$–$Si_{1,1}$	$M_{1,1}$–$PSi2_{1,1}$	0.00	− 0.10
	41	$M_{1,1}$–$Si_{1,1}$	$M_{1,1}$–$PSi2_{2,1}$	0.00	− 0.05
	42	$M_{1,1}$–$PSi1_{1,1}$	$M_{1,1}$–$PSi1_{2,1}$	0.00	0.05
	43	$M_{1,1}$–$PSi1_{1,1}$	$M_{1,1}$–$PSi2_{1,1}$	0.15	0.15
	44	$M_{1,1}$–$PSi1_{1,1}$	$M_{1,1}$–$PSi2_{2,1}$	0.15	− 0.05
	45	$M_{1,1}$–$PSi2_{1,1}$	$M_{1,1}$–$PSi2_{2,1}$	0.00	0.05
Si	46	$M_{1,1}$–$Si_{1,1}$	$Si_{1,1}$–$Si_{2,1}$	0.10	0.00
(tetrahedral)	47	$M_{1,1}$–$Si_{1,1}$	$Si_{1,1}$–$PSi1_{1,2}$	0.00	0.00
	48	$M_{1,1}$–$Si_{1,1}$	$Si_{1,1}$–$PSi2_{1,2}$	0.00	0.00
	49	$Si_{1,1}$–$Si_{2,1}$	$Si_{1,1}$–$PSi1_{1,2}$	0.00	0.00
	50	$Si_{1,1}$–$Si_{2,1}$	$Si_{1,1}$–$PSi2_{1,2}$	0.00	0.00
PSi1	51	$Si_{1,1}$–$PSi1_{1,2}$	$Si_{1,1}$–$PSi2_{1,2}$	− 0.05	− 0.30
(tetrahedral)	52	$M_{1,1}$–$PSi1_{1,1}$	$Si_{1,1}$–$PSi1_{1,2}$	− 0.20	0.00
	53	$M_{1,1}$–$PSi1_{1,1}$	$PSi1_{1,1}$–$PSi1_{2,1}$	0.00	0.00
	54	$M_{1,1}$–$PSi1_{1,1}$	$PSi1_{1,1}$–$PSi2_{2,2}$	0.00	0.00
	55	$Si_{1,1}$–$PSi1_{1,2}$	$PSi1_{1,1}$–$PSi1_{2,1}$	0.00	0.00
	56	$Si_{1,1}$–$PSi1_{1,2}$	$PSi1_{1,1}$–$PSi2_{2,2}$	0.20	0.00
	57	$PSi1_{1,2}$–$PSi1_{2,1}$	$PSi1_{1,1}$–$PSi2_{2,2}$	− 0.10	0.00
PSi2	58	$M_{1,1}$–$PSi2_{1,1}$	$Si_{1,1}$–$PSi2_{1,2}$	0.00	0.00
(tetrahedral)	59	$M_{1,1}$–$PSi2_{1,1}$	$PSi1_{2,1}$–$PSi2_{1,2}$	− 0.10	0.00
	60	$M_{1,1}$–$PSi2_{1,1}$	$PSi1_{1,1}$–$PSi2_{2,1}$	0.00	0.07
	61	$Si_{1,1}$–$PSi2_{1,2}$	$PSi1_{2,1}$–$PSi2_{1,2}$	0.00	0.00
	62	$PSi2_{1,1}$–$PSi2_{2,1}$	$PSi1_{1,1}$–$PSi2_{2,1}$	0.00	0.00
	63	$Si_{1,1}$–$PSi2_{2,1}$	$PSi1_{2,1}$–$PSi2_{1,2}$	− 0.10	0.00

orthogonal to the **b** axis. Very similar force constants equal to 1.40 and 1.43 Nm^{-1} correspond to these bonds. However, bond number 8 connects two octahedra located in two different planes perpendicular to the **b** axis and the associated force constant is very different (1.79 instead of 1.40 and 1.43 Nm^{-1} for bond 7 and 9). Thus, stretching force constants do not follow usual correlations between interatomic distances and force constants (17) unlike most ionocovalent compounds. The same conclusion can also be made in the Rh compound. In the present case, because of the delocalization of electrons, one must consider that the force constants do not have the same chemical meaning as for ionic or molecular crystals in which electrons responsible for the bond are localized on or between atoms defining the bond. In this respect, it can be noticed that the coordination polyhedra are rather distorted in both compounds and the bonds do not fit the sum of atomic or ionic radii (18).

Atomic motions (*LX*). We have studied the atomic displacements for each vibrational mode. For most of them, the interpretation of these displacements in terms of motions of an isolated octahedron, such as the well-known "breathing" motion, is not possible. In fact, octahedra are linked together by Si–Si, Si–P, or P–P bonds whose strengths are comparable to those of octahedron internal bonds. Furthermore, the calculated stretching force constants for these bonds are close to those of *M*–Si or *M*–P bonds (see Table 2). Thus, the displacements of an octahedron are strongly coupled to its neighbors giving rise to tridimensional framework motions. In addition, the atomic displacements of PSi1 and PSi2 are often very similar, as expected from the pseudo-centrosymmetry. This can be seen in Figs. 5a and 5b. This figure shows the atomic displacements for the 495 cm^{-1} *B* mode and the 554 cm^{-1} *A* mode for which the PED shows the predominance of the PSi1–PSi2 internal coordinate. In both cases, the largest atomic displacements are for PSi1 and PSi2 and correspond to PSi1–PSi2 stretching modes.

CONCLUSION

These results show that the analysis of vibrational spectra is a very good complement to the X-ray diffraction study to

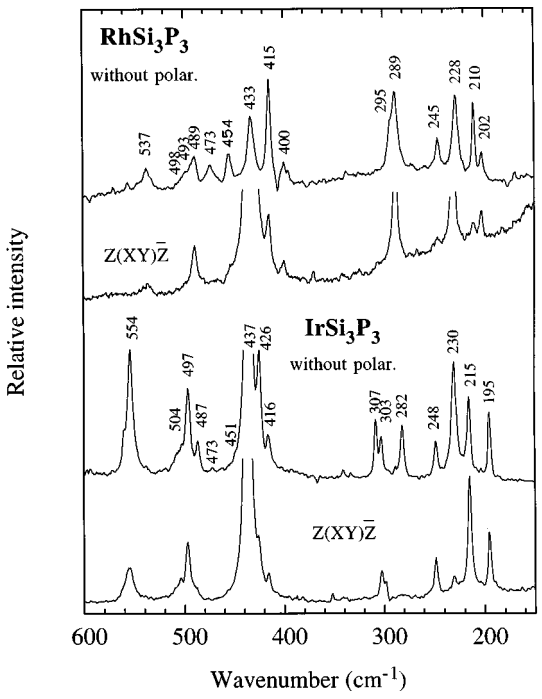

FIG. 3. Polarized and unpolarized Raman spectra of $RhSi_3P_3$ and $IrSi_3P_3$.

distinguish between centrosymmetric and noncentrosymmetric groups. All of the 18 Raman-active optical modes expected in the $C2$ (or C_2^3) space group have been observed in the spectra. This unambiguously attests to a noncentrosymmetric structure.

The differences between wavenumbers in $IrSi_3P_3$ and $RhSi_3P_3$ spectra are too small to be explained by a simple mass effect, as in the isotopic substitution case. Actually, $IrSi_3P_3$ force constants are larger than those of $RhSi_3P_3$ force constants, while the bond lengths are quite similar in both compounds.This could indicate that electrons are not as delocalized for $IrSi_3P_3$ as for $RhSi_3P_3$.

From the analysis of the potential energy distribution, it can be seen that the modes can be distributed among three groups of wavenumbers which involve the same type of internal coordinates and that some of them are strongly localized.

The differences between force constants for internal coordinates associated to bonds of the same nature and of the same length can be explained by a delocalization of the electrons. The anisotropy of PSi–PSi force constants is more pronounced for $IrSi_3P_3$. This is in agreement with an electronic delocalization which is less marked for the Ir compound.

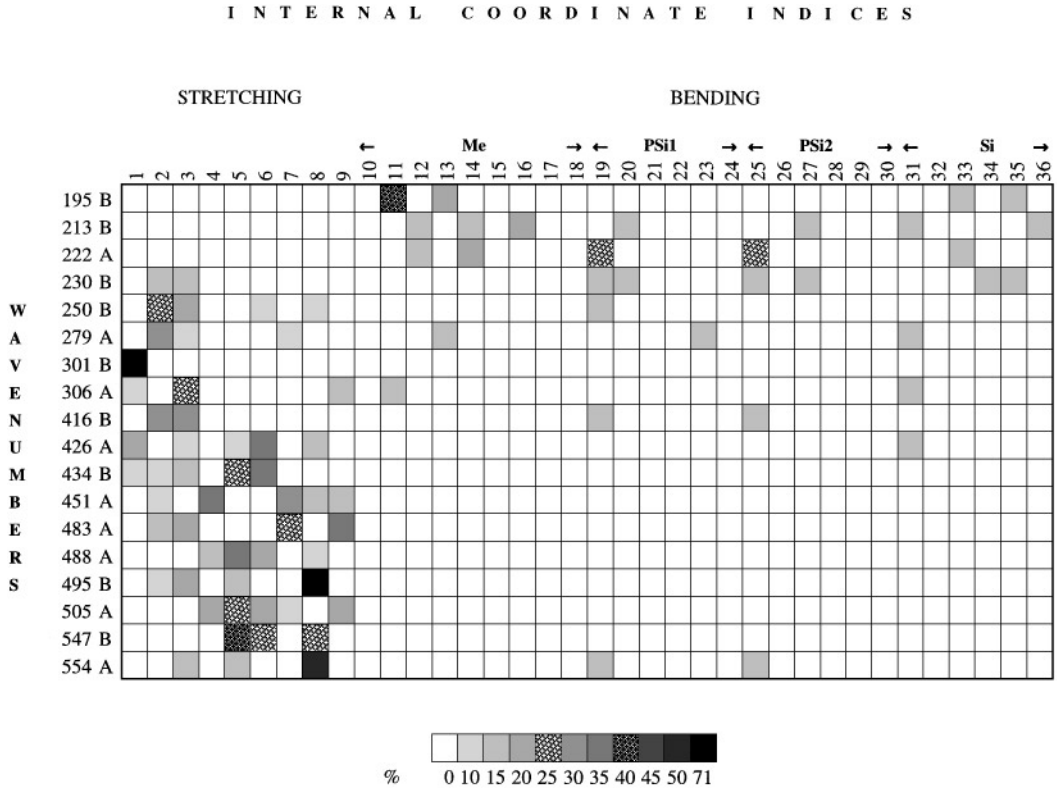

FIG. 4. Schematic representation of the potential energy distribution of $IrSi_3P_3$ from the principal (diagonal) force constants.

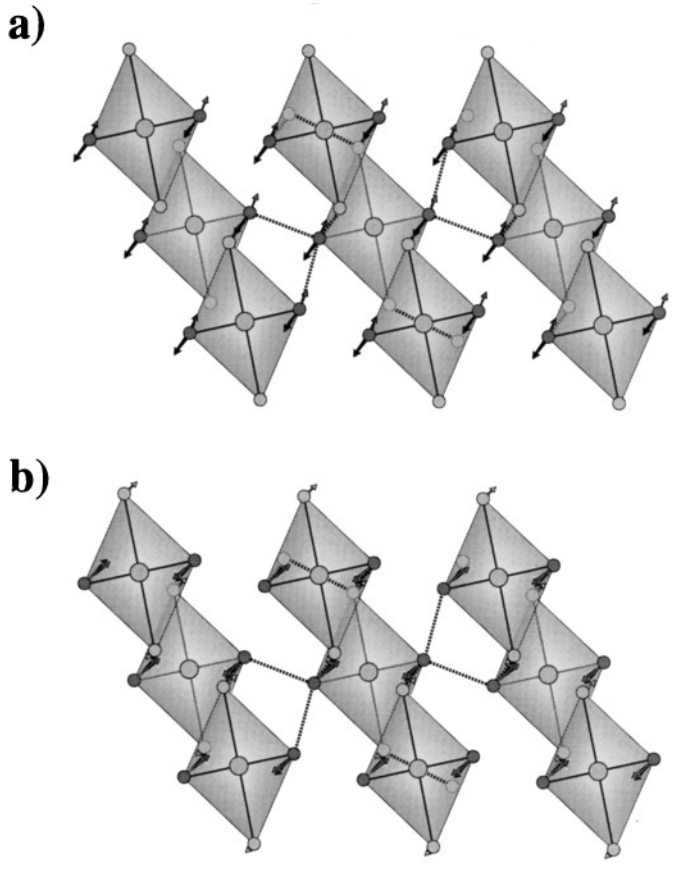

FIG. 5. Cartesian displacements of the atoms for $IrSi_3P_3$ (projection parallel to [010]): B 495 cm^{-1} mode (**a**) and A 554 cm^{-1} mode (**b**). In both cases, the most stretched motions of PSi1–PSi2 bonds are mainly involved (internal coordinates 8,1 and 8,2 superimposed on the figures).

REFERENCES

1. B. Aronsson, T. Lundström and S. Rundquist, "Borides, Silicides and Phosphides," Methuen, London, 1965.
2. F. Nava, E. Mazzega, M. Michelini, O. Laborde, U. Gottlieb, O. Thomas, J. P. Senateur, and R. Madar, *J. Appl. Phys.* **65,** 1584 (1989).
3. M. Kirschen, H. Vincent, Ch. Perrier, P. Chaudouët, B. Chenevier, and R. Madar, *Mater. Res. Bull.* **30,** 507 (1995)
4. Ch. Perrier, H. Vincent, P. Chaudouët, B. Chenevier, and R. Madar, *Mater. Res. Bull.* **30,** 357 (1995).
5. H. Vincent, J. Kreisel, Ch. Perrier, O. Chaix-Pluchery, P. Chaudouët, R. Madar, F. Genet, and G. Lucazeau, *J. Solid State Chem.* **124,** 366 (1996).
6. H. Vincent, Ch. Perrier, M. Kirschen, and R. Madar, "11th ICSCTE," Wroclaw, Pologne, 1994.
7. M. Amiotti, A.Borghesi, G. Guizzetti, F. Nava, and G. Santoro, *Europhys. Lett.* **14,** 587 (1991).
8. A. Borghesi, A. Piaggi, A. Franchini, G. Guizzetti, F. Nava, and G. Santoro, *Europhys. Lett.* **11,** 61 (1990).
9. O. Chaix-Pluchery, L. Abello, G. Lucazeau, B. Chenevier, and R. Madar, *J. Phys. Chem. Solids.* **57,** 527 (1996).
10. O. Chaix-Pluchery, F. Genet, G. Lucazeau, and R. Madar, *Appl. Surf. Sci.* **91,** 68 (1995).
11. K. Lefki, P. Muret, E. Bustarret, N. Boutarek, R. Madar, J. Derrien, and M. Brunel, *Solid State Commun.* **80,** 791 (1990).
12. L. Fayette, B. Marcus, M. Mermoux, N. Rosman, L. Abello, and G. Lucazeau, *J. Appl. Phys.* **76,** 1604 (1994).
13. N. Walker and D. Stuart, *Acta Crystallogr. A* **39,** 158 (1983).
14. "International Tables for Crystallography A," Kluwer Academic, Dordrecht/Boston/London, 1989.
15. E. B. Wilson, J. C. Decius, and P. C. Cross, "Molecular vibrations." Mc Graw-Hill, New York/Toronto/London, 1955.
16. F. Genet, "Program NORMOD," to be published.
17. F. Genet, S. Loridant, and G. Lucazeau, submitted for publication
18. Ch. Perrier, Thesis, Institut National Polytechnique de Grenoble, France, 1995.